THE JOURNAL OF PHYSICAL CHEMISTRY C

Article

pubs.acs.org/JPCC

Are 4-Mercaptobenzoic Acid Self Assembled Monolayers on Au(111) a Suitable System to Test Adatom Models?

E. Pensa,[†] A. A. Rubert,[†] G. Benitez,[†] P. Carro,[‡] A. González Orive,[‡] A. Hernández Creus,[‡] R. C. Salvarezza,[†] and C. Vericat[†,*]

[†]The Research Institute of Theoretical and Applied Physical Chemistry (INIFTA) Faculty of Exact Sciences, National University of La Plata - CONICET-Sucursal 4 Casilla de Correo 16, (1900) La Plata, Argentina

[‡]Departament of Physical Chemistry, Institute of Materials and Nanotechnology (IMN), University of La Laguna, Avda. Astrofísico Francisco Sánchez S/N, La Laguna 38071, Tenerife, Spain

ABSTRACT: The adsorption of 4-mercaptobenzoic acid (MBA) has been studied on Au(111) by scanning tunneling microscopy (STM), X-ray photoelectron spectroscopy (XPS), electrochemical techniques, and density functional theory (DFT) calculations. Results show that MBA molecules adsorb on the Au surface via a thiolate bond, arranged in a $(\sqrt{3}\times4)$ lattice with coverage θ_{RS} = 0.25. DFT data show the strong effect of aromatic ring interactions in stabilizing the adsorbed molecules. The total absence of vacancy islands upon thiol adsorption and the surface coverage of gold islands after desorption are difficult to conciliate with the usual gold-adatom models for thiol adsorption. This is an important issue, as the strongest evidence for the existence of gold-adatom complexes arises from MBA-capped Au nanoparticles. Our results raise an interesting point as regards the validity of making a straightforward parallel between the thiol−Au interface in single crystal surfaces and in monolayer-protected clusters.

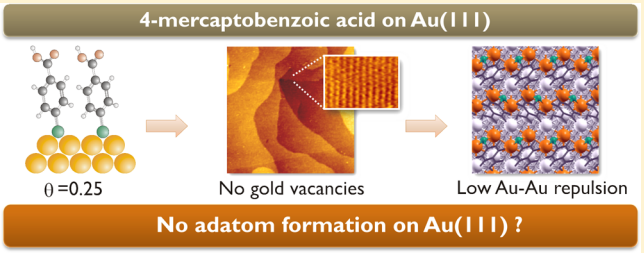

INTRODUCTION

Since their discovery in the early 1980s,[1] self-assembled monolayers (SAMs) of thiols on gold (and on other metals as well) have been increasingly used as both a structural and functional part in nanotechnological applications like sensors and biorecognition systems, molecular electronic devices, drug-delivery systems, and protecting capping for nanostructures, just to mention a few examples.[2] These SAMs can be regarded as insulator layers of controlled thickness and are a versatile and robust linker of different species (macromolecules, clusters and nanoparticles, antibodies, etc.) to the metal surface.[3]

Alkanethiol SAMs on the (111) gold surface have been established as a model system in modern surface science.[4,5] They have been (and are still) studied by many groups around the globe by using every possible surface science technique. Alkanethiols yield ordered, commensurate lattices on Au(111), the most usual being the $(\sqrt{3}\times\sqrt{3})$-R30° and its related c(4×2) superlattice, which can coexist on the same surface. These dense lattices have thiolate surface coverage θ_{RS} = 0.33 and nearest-neighbor thiol−thiol distances $d \approx 0.5$ nm. One of the most remarkable features of these SAMs, when studied by scanning tunneling microscopy (STM), are the "pits" or vacancy islands that are formed during thiol adsorption and whose depth is equivalent to the height of one or two gold layers.[6] The origin of these vacancies, systematically observed for all alkanethiol SAMs irrespective of their length, has been a long-time controversial issue.

In the early 2000s, the picture of a simple organized monolayer on the unreconstructed Au(111) surface, though still with some unanswered questions, like the origin of the c(4×2) lattice, or the nature of the "pits", was certainly challenged by the dissimilar results arising from density functional theory (DFT) calculations[7−9] and, more important, by a couple of experimental results from synchrotron diffraction techniques.[10,11]

Since then, and up to present, the so-called adatom models, which imply a considerable reconstruction of the Au(111) surface, have aroused great interest and provoked not little controversy.[4,12−15] This new picture of the S−Au interface, which is based on the formation of some kind of gold−thiolate complex, the most important being the RS-Au and RS-Au-SR species,[13,14] gives a reasonable explanation for the existence of the gold vacancy islands. In fact, it is now accepted that a certain amount of gold atoms are removed from the topmost layer (or top two layers) of the gold surface to form the gold−thiolate complexes, thus leaving monatomic vacancies that yield larger vacancy islands by Ostwald ripening. Indeed, the gold vacancy island coverage (θ_{vac}), calculated from the analysis of many STM images, has been regarded as an indirect evidence of the presence of adatoms on the Au(111) surface.

Received: July 2, 2012
Revised: October 10, 2012
Published: December 4, 2012

Among the numerous adatom models proposed, the one that is most widely accepted is that proposed by Grönbeck et al., which involves RS-Au-SR units in a cis configuration (the $(RS)_2Au$ model).[14] This model shows the highest thermodynamical stability in terms of the free energy, as calculated by DFT. Moreover, because the thiolate coverage θ_{RS} is 0.33, according to this model the adatom coverage should be 0.165. This value is close to that found from STM imaging both for the experimental θ_{vac} value and for the coverage of gold islands that are formed on the (111) terraces after complete thiol desorption.[5]

The success of the $(RS)_2Au$ model is also due to the fact that it provided a unified view of the gold−thiolate interface for both planar (111) surfaces and gold nanoclusters.[14,16] The structural determination by X-ray diffraction of a Au_{102} cluster capped with 44 4-mercaptobenzoic acid (MBA) molecules was a key element in the success of the $(RS)_2Au$ model for the Au(111) surface, because the former consists of 79 Au atoms covered by 19 of the RS-Au-SR units and 2 additional $RS(AuSR)_2$ species.[17,18] The bottom line was therefore that the RS-Au-SR complexes provided a unified picture of thiolate bonding to gold surfaces, irrespective of their curvature.[14]

MBA SAMs on Au(111) have been previously studied by IR techniques,[19,20] cyclic voltammetry (CV),[21] X-ray photoelectron spectroscopy (XPS)[20,22] and STM,[23] among others. However, even if this was the thiol of choice for some of the seminal studies about the structure of gold clusters that lead to the unified model of the thiol−gold interface,[5] little is known about the structure and the chemistry of the interface of MBA SAMs on Au(111) in the light of the new adatom models.

In this work we have studied MBA SAMs on Au(111) in air by STM (together with XPS and CV to determine the thiol coverage) and have performed DFT calculations considering van der Waals interactions. In contrast to what is usually found for alkanethiol SAMs on Au(111), STM results show the total absence of vacancy islands on the terraces and a small number of islands on the surface after complete thiol desorption, similar to what has been previously observed for other aromatic thiols.[24,25] High resolution imaging yields a lattice that agrees well with the obtained surface coverage and which was used to model the slab for DFT. Calculations reveal that a possible cause for the lack of adatoms lies in the small charge on the surface gold atoms after charge transfer with the adsorbate.

Our results for MBA on Au(111) seem to be inconsistent with the formation of gold adatoms from terraces upon thiol adsorption, a necessary step to account for the proposed models of the unified thiolate−gold interface. This raises an interesting point as regards the validity of making a straightforward parallel between the thiol−Au interface in single crystal surfaces and in monolayer protected clusters.

MATERIALS AND METHODS

Experimental Procedure. 4-Mercaptobenzoic acid (MBA) (Aldrich, 90%), NaOH (Sigma, 98.6%), and absolute ethanol (Carlo Erba, 99.5%) were used as received. Evaporated Au films on glass with (111) preferred orientation (AF 45 Berliner Glass KG, Germany) were used as substrates. After annealing for 3 min with a hydrogen flame, these Au substrates exhibit atomically smooth (111) terraces separated by steps of monatomic height, as revealed by scanning tunneling microscopy (STM).

MBA SAMs were formed on the Au(111) substrates by immersion of the clean substrates in deaerated 100 μM MBA ethanolic solutions for 30 min. Then, the samples were removed from the solution, rinsed with the solvent, dried with N_2 and imaged in air by STM, immediately placed in the UHV chamber for XPS (X-ray photoelectron spectroscopy) analysis, or placed in the electrochemical cell for voltammetry. Experiments were also made in the same solvent but with longer incubation times (12 and 24 h). In all cases the same results were obtained by all the used techniques. The shortest incubation time (30 min) was chosen for practical reasons.

Special care was taken for sample preparation for XPS measurements. In those cases rinsing was made with copious amounts of absolute ethanol.

Scanning Tunneling Microscopy Measurements. In air STM experiments were performed in the constant current mode with an ECM microscope from Veeco Instruments (Santa Barbara, CA) controlled by a Nanoscope IIE unit, also from Veeco Instruments. Mechanically cut Pt−Ir tips were used and typical bias voltages (E_{bias}), set point currents, and scan rates were −0.3 to +0.5 V, 0.1−0.5 nA, and 1−30 Hz, respectively. The scanner calibration was checked by imaging highly oriented pyrolytic graphite (HOPG) with atomic resolution.

X-ray Photoelectron Spectroscopy. XPS measurements were performed with a Mg Kα source (XR50, Specs GmbH) and a hemispherical electron energy analyzer (PHOIBOS 100, Specs GmbH) operating at 10 eV pass energy. A two-point calibration of the energy scale was performed using sputtered cleaned gold (Au $4f_{7/2}$, binding energy = 84.00 eV) and copper (Cu $2p_{3/2}$, binding energy = 932.67 eV) samples. C 1s at 285 eV was used as charging reference. Spectra were analyzed with CasaXPS v2.3.14 and XPS Peak 4.1 software packages. A Shirley-type background was used to fit each spectrum. The fitting of the S 2p (Au 4f) peaks was carried out by using a spin−orbit splitting of 1.19 eV (3.65 eV) and a branching ratio of 0.5 (0.75).

Electrochemical Measurements. Cyclic voltammetry was performed with a potentiostat with digital data acquisition (TEQ, Argentina). The thiol-modified Au(111) substrate (working electrode) was mounted in a conventional three-electrode glass cell using a Pt large area wire as counter and a saturated calomel electrode (SCE) as reference electrodes, respectively. Aqueous 0.1 M NaOH solutions were prepared by using deionized H_2O from a Milli-Q purification system (Millipore Products, Bedford) which were degassed with purified nitrogen prior to the experiments.

Thiol reductive electrodesorption was performed by scanning the potential from −0.3 to −1.4 at 0.1 V s^{-1} in the 0.1 M NaOH solution at room temperature. In each case the charge density involved in the reductive desorption (calculated by integration of the peak area and taking into account the electrode real area from the gold oxide reduction peak) was taken as an indication of the surface coverage by the SAM. Results are an average of more than 10 measurements.

Density Functional Theory Calculations. First principle calculations were performed using the Vienna ab initio simulation package (VASP) based on plane-wave pseudopotential periodic DFT. The electron-ion interactions were described by the projector augmented wave (PAW) method,[26,27] as implemented by Kresse and Joubert.[28] The exchange−correlation potential was described by means of the generalized gradient approach (GGA) with the Perdew−Wang (PW91)[29] implementation. The one-electron wave functions were expanded on a plane wave basis set with an

energy cutoff of 520 eV. The Brillouin zone sampling was carried out according to the Monkhorst–Pack[30] scheme with (9 × 4 × 1) dense *k*-points meshes. The energy minimization (electronic density relaxation) for a given nuclear configuration was carried out using a Davidson block iteration scheme. The dipole correction was applied to minimize polarization effects caused by asymmetry of the slabs. All calculations have been carried out using the VASP 5.2 package.[28,31] To take into account the dispersion effects present in organic compounds, calculations have been undergone including van der Waals corrections realized with the Grimme approach.[32] In this method a semiempirical dispersion potential is added to the conventional Kohn–Sham DFT energy ($E_{KS\text{-}DFT}$) according to (1)

$$E_{DFT\text{-}D} = E_{KS\text{-}DFT} + E_{dispersion} \quad (1)$$

where the dispersion energy ($E_{dispersion}$) is calculated for all the atoms in the unit cell. The cutoff radius for pair interactions used is 12 Å. Thus, the van der Waals interactions of the carboxyl groups are also included in the energy value.

The surface periodic slab was modeled in a $(\sqrt{3}\times4)$ surface cell composed of five metal layers and a vacuum of ~12 Å and two moieties per unit cell. Adsorption occurs only on one side of the slab. During the geometry optimization the two bottom layers were kept fixed at their optimized bulk truncated geometry for the Au(111) surface. The three outermost atomic metal layers, as well as the atomic coordinates of the adsorbed species, were allowed to relax without further constraints. The atomic positions were relaxed until the force on the unconstrained atoms was less than 0.03 eV Å^{-1}. The lattice parameter calculated for bulk Au was 4.18 Å, in good agreements with the experimental value (4.078 Å).[33]

We define the average binding energy per MBA adsorbed radical (E_b) as follows,

$$E_b = \frac{1}{N_{MBA^\bullet}}[E^{MBA^\bullet/Au} - E^{Au} - N_{MBA^\bullet}E_{MBA^\bullet}] \quad (2)$$

where $E^{MBA^\bullet/Au}$, E^{Au}, $E_{MBA^\bullet}$, and $N_{MBA^\bullet}$ stand for the total energy of the system, the energy of the clean surface, the energy of the adsorbed radical that results when MBA loses the hydrogen atom of the S–H group, and the number of MBA species per unit cell, respectively. Negative numbers indicate an exothermic adsorption process with respect to the clean surface and the adsorbed phase originated during the adsorption process.

RESULTS AND DISCUSSION

High resolution XP spectra are shown in Figure 1 for MBA SAMs on Au(111). The Au 4f region can be fitted with one component with Au4f$_{7/2}$ BE = 84.0 eV, which corresponds to metallic gold. On the other hand, the S 2p region can be also fitted with a single S 2p$_{3/2}$ component at BE = 162.0 eV, which is attributed to the formation of a thiolate bond on Au(111). A second component at ≈163 eV is sometimes found that corresponds to unbounded thiols and which depends on, among other factors, the rinsing procedure. It is important to stress that there are no traces of sulfide impurities in our spectra, which would yield a peak at BE ≈ 161 eV. Moreover, they show no components at BE > 164 eV, indicating the absence of oxidized S species (sulfonates, sulfates, etc.) on the Au surface.

Therefore, we can conclude that practically all molecules are chemisorbed on the gold surface, and that the S/Au intensity

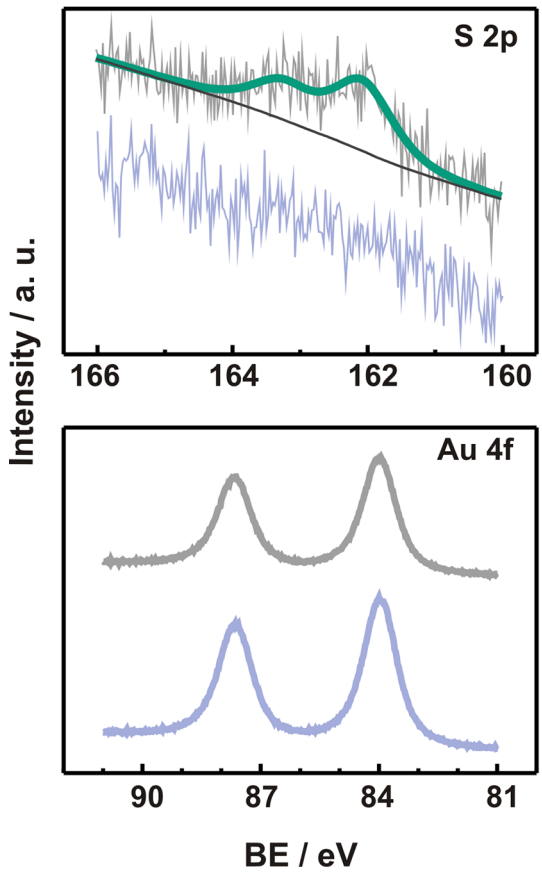

Figure 1. High resolution XP spectra of the S 2p (upper) and Au 4f (lower) regions for MBA SAMs on Au(111). Both the S 2p and the Au 4f regions can be fitted with a single component at 162.0 eV (green line) and at 84.0 eV (red line), respectively. The blue spectra in each panel show the corresponding S 2p and Au 4f signals after the reductive desorption procedure described in Figure 2.

ratio (corrected for the sensitivity factors) corresponds to a surface coverage θ_{RS}= 0.25.

In Figure 2, cyclic voltammograms (CVs) recorded at 0.1 V s^{-1} in 0.1 M NaOH are shown for MBA SAMs formed by

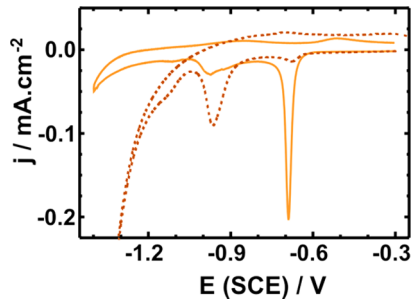

Figure 2. Cyclic voltammograms of 4-mercaptobenzoic acid SAMs on Au(111) (orange full line) and on polycrystalline Au (brown dotted line). Immersion was performed for 30 min in ethanolic solutions. Scan rate: 0.1 V s^{-1}. Electrolyte: 0.1 M NaOH.

immersion of Au(111) and polycrystalline gold substrates for 30 min in the MBA solution. The orange full line shows a CV of the reductive desorption region of the adsorbate for a Au(111) substrate. Only a small amount of thiolates are readsorbed in the anodic scan, indicating that most of these species diffuse away from the surface. The most important

dx.doi.org/10.1021/jp306545v | J. Phys. Chem. C 2012, 116, 25765–25771

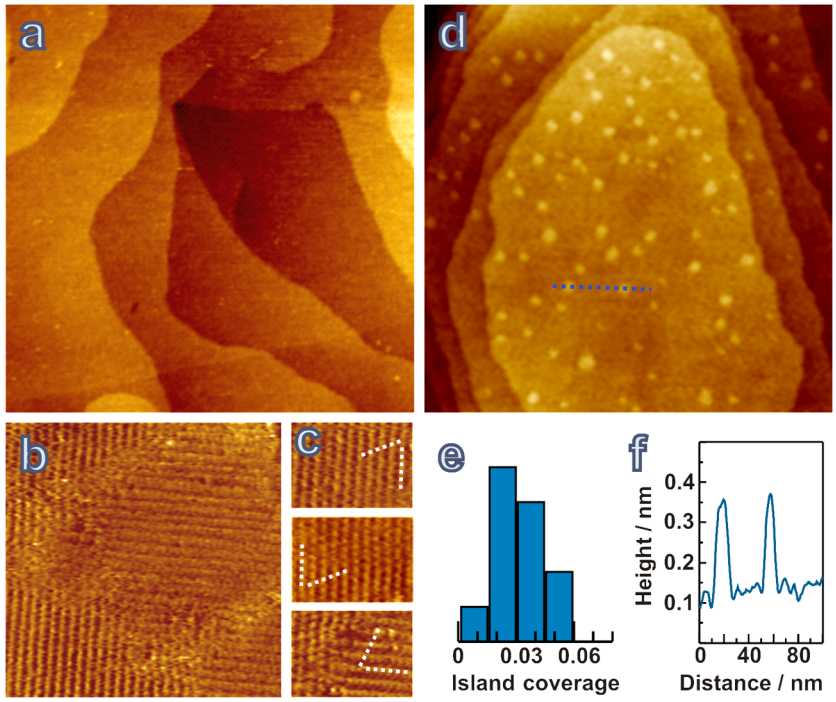

Figure 3. In air STM images and related data of MBA on Au(111) before (a)−(c) and after (d)−(f) complete thiol electrodesorption. Incubation time of the Au(111) in the MBA solution was 30 min. (a) 300 × 300 nm^2 image showing total absence of vacancy islands upon MBA adsorption on the substrate. (b) 17 × 17 nm^2 high resolution image of MBA domains. (c) Three images (5 × 7 nm^2) with molecular resolution showing the surface structure of the adsorbate on Au(111), which can be described in terms of a ($\sqrt{3}$×4) lattice. The angle between nonequivalent MBA radicals is about 66°. White lines were drawn to guide the eye. (d) 300 × 300 nm^2 image of the substrate surface after the electrochemical desorption of MBA. Gold islands can be imaged. (e) Histogram of the surface coverage of gold islands (more than 10 images were analyzed). (f) Cross section showing the height of the gold islands (corresponding to the blue dash line in (d)).

cathodic current peak appears at −0.68 ± 0.01 V and has a charge density 57 ± 8 μC cm^{-2}. This corresponds to a surface coverage θ_{RS} = 0.25, consistent with the coverage obtained from our XPS measurements and with previously reported data.[34] Moreover, a smaller peak at ca. −0.98 V, with a charge density 15 ± 3 μC cm^{-2}, can be observed in all voltammograms. The same value (θ_{RS} = 0.25) was obtained after a 24 h immersion, indicating that the saturation coverage is already attained in 30 min. Because there are no traces of sulfide species (which are desorbed at similar potentials under the same experimental conditions) in the 2p region in the XP spectra (Figure 1), we believe that the smaller cathodic peak is due to the desorption of MBA molecules from gold crystalline faces other than the (111), as previously reported by Ohsaka et al.[21] To confirm this fact for our own experimental conditions, electrochemical desorption of MBA SAMs on polycrystalline Au substrates has been performed (brown dotted line in Figure 2). In this case, two desorption peaks appear at the same potentials as for Au(111), although here the peak at ≈−0.98 V is predominant, thus confirming our hypothesis. It should be stressed, however, that for our substrates the largest contribution comes from the gold (111) crystalline face.

Figure 3 shows different in air STM images of MBA SAMs on Au(111) taken under controlled humidity conditions. In Figure 3a, a typical large-area image (300 × 300 nm^2) shows atomically flat terraces which, in contrast to those observed for alkanethiol SAMs,[5] are completely free of vacancy islands. The same result was found after 24 h incubations of the Au(111) substrates. This important fact has been concluded from the analysis of more than 25 images of at least 6 samples, all free from sulfide contamination. Schäfer et al. had already mentioned the absence of the vacancy islands typical of alkanethiol SAMs on Au(111) and the presence of "disordered areas" in their STM images.[23] A complete lack of vacancy islands on (111) gold terraces as a result of the self-assembly of a thiol on Au(111) has been previously found in our group for 6-mercaptopurine on Au(111),[24] though in this case some monatomic high gold islands were also present. A mixture of gold islands and of vacancy islands has been reported for several aromatic thiols on Au(111).[35,36]

Figure 3b shows a higher resolution image (17 × 17 nm^2) with ordered MBA domains. As with other carboxylic acid-terminated thiols, due to the hydrophilic nature of these groups it is important to image samples under low humidity conditions. Otherwise, a layer of water tends to form on the SAM, making STM imaging difficult. Four domains of a striped pattern of bright spots can be clearly observed. The dark features observed in the central domain in Figure 3b have a much lower depth (0.08 nm) than 0.24 nm. Thus, it is clear that they are not gold vacancy islands but probably regions of missing (or disordered) molecules, or regions where tunneling was not achieved.

The periodic structure has been better defined in the high resolution images in Figure 3c, although it is clear that some disorder is present in this lattice. The typical nearest neighbor distance between adjacent stripes is 0.65 ± 0.07 nm, and the angle (marked in the images with white dotted lines) is 66 ± 3°. The short distance in the lattice cannot be precisely determined, though it is between 0.4 and 0.5 nm. This surface structure was also found when imaging SAMs formed after 24 h

dx.doi.org/10.1021/jp306545v | J. Phys. Chem. C 2012, 116, 25765−25771

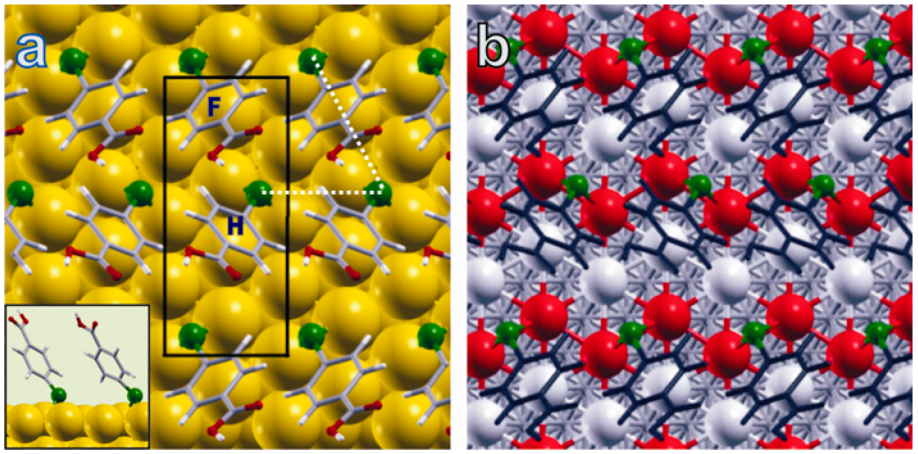

Figure 4. (a) Top view of the optimized surface structure of the ($\sqrt{3}$×4) MBA lattice on the unreconstructed Au(111) surface, with two molecules per unit cell, one in bridge-fcc (F) and the other in bridge-hcp (H) position. Color: yellow, Au; green, S; gray, C; white, H; red, O atoms. The unit cell is marked by a black box. Dotted white lines point out the angle outlined in Figure 3c. The inset shows a side view of the surface structure. (b) Schematic representation of Bader charges of the topmost Au surface atoms. Color: white, negative charge; red, positive charge.

incubation (data not shown). The observed distances are shorter than those previously reported by Schäfer et al. for MBA on the Au(111) surface.[23] From the STM images and taking into account the coverage obtained from CV and XPS measurements we can describe the thiol lattice in terms of a ($\sqrt{3}$×4) unit cell with two molecules (θ_{RS} = 0.25).

The coverage of vacancy islands on terraces has been taken as a strong evidence of the formation of either RS-Au-SR or RS-Au moieties. For alkanethiol dense lattices the vacancy coverage should be either 0.165 or 0.33, for the $(RS)_2Au$ or the RSAu model, respectively. Clearly, the number of gold adatoms needed largely exceeds that arising from the lifting of the 22×$\sqrt{3}$ Au(111) reconstruction (θ_{adatom} = 0.05) induced by thiol adsorption.[5] This means that, to account for a dense SAM, an additional number of adatoms equivalent to $\theta_{adatom} \approx 0.11$ or ≈0.28 is needed, which should be taken from the Au(111) surface. The absence of vacancy islands suggests that RS-Au-SR or RS-Au moieties are not present on the Au(111) surface. However, this result is not conclusive, as adatoms could arise from step edges where a smaller energy for atom removal is needed.

To gain evidence about the amount of adatoms on the Au(111) surface and the nature of the possible thiolate−Au-adatom species, the Au substrates were also imaged by STM after complete thiol desorption, which was accomplished by reductive electrodesorption in an electrochemical cell. Several cycles were needed to completely remove the thiol from the surface, as checked by XPS (see the spectra in blue in the two panels in Figure 1). The terraces show some gold islands of monatomic height (0.24 nm, see Figure 3d,f), as observed for alkanethiols[5,24,37] and for 6-mercaptopurine.[24] From the analysis of the images a histogram of the island coverage has been made, which shows a maximum for θ_{isl} = 0.02 (Figure 3e). This value is similar to that observed for 6-mercaptopurine SAMs on Au(111). As speculated before,[24] the small number of gold islands can arise from the lifting of the 22×$\sqrt{3}$ Au(111) reconstruction (θ_{isl} = 0.05).[38] Therefore, for MBA SAMs the experimental gold island coverage is not compatible with the presence of either RS-Au-SR or RS-Au species, for which the island coverage after MBA desorption should be $\theta_{isl} \approx 0.125$ and 0.25, respectively. Again, it could be argued that mobile Au adatoms can be captured at step edges, thus yielding a much lower gold island density. However, the Schwoebel−Ehrlich barrier to gold-adatom incorporation at a step of a lower terrace is high, and thus adatom incorporation into these steps is improbable.[39] Therefore, the coverage by Au islands of the upper large terrace in Figure 3d should reflect the total amount of Au adatoms present in the MBA SAM. Moreover, it is well-known that gold islands are indeed observed after the lifting of the 22×$\sqrt{3}$ Au(111) reconstruction, a process that also results in the formation of mobile Au adatoms (although a much smaller adatom population is involved compared to the desorption of thiol SAMs for which thiolate-adatom models apply).[38]

DFT calculations have been employed to explore the energetic and structural characteristics of MBA SAM on Au(111). On the basis of the STM observations, an unreconstructed (111) surface was modeled and the unit cell proposed was the ($\sqrt{3}$×4) with two MBA radicals oriented along the $[11\bar{2}]$ and $[1\bar{2}1]$ directions, with θ_{RS} = 0.25. We have found that in the most stable configuration the MBA species are bonded with the S atom located on bridge-fcc hollow (F) and bridge-hcp hollow (H) sites, respectively, as found in previous calculations for alkanethiolates on the unreconstructed Au(111) surface. Results show that both MBA species adsorb in a standing up configuration with the molecular axis tilted 37.4° (bridge-hcp) and 33° (bridge-fcc) with respect to the surface normal, in agreement with experimental data.[22] The optimized surface structure is shown in Figure 4a. Distances between nearest neighbor MBA radicals are 0.51 and 0.64−0.65 nm, in good agreement with the STM images shown in Figure 3. A summary of the structural and energetic parameters obtained for the optimized configuration is presented in Table 1. It is evident that the binding energy of the thiolate species adsorbed on the Au(111) surface is largely improved by including van der Waals (vdW) interactions between adjacent aromatic rings in the calculations. In fact, vdW interactions add an additional −0.71 eV to the binding energy, a value close to that estimated for benzenethiol,[5] thus stabilizing the surface structure. The van der Waals interactions have not significant influence on the structural parameters, as seen in Table 1. However, one can appreciate slightly shorter Au−S distances and the molecular axis more tilted to the surface when the long-range interactions are included. A Bader charge analysis of the

dx.doi.org/10.1021/jp306545v | J. Phys. Chem. C 2012, 116, 25765−25771

Table 1. Structural and Energetic Parameters Obtained for the Optimized Configuration of a MBA SAM on an Unreconstructured Au(111) Surface[a]

	Energetic and Structural Data			
	without vdW		with vdW	
	MBA_F	MBA_H	MBA_F	MBA_H
tilt angle (α)/deg	32.5	36.3	33.0	37.4
S–Au bond	2.52	2.53	2.50	2.54
length/Å	2.52	2.47	2.50	2.44
E_b/eV	−1.39		−2.10	
	Bader Charges/e			
	without vdW		with vdW	
$Au_{topmost}$	+0.02		+0.02	
S_F	−0.13		−0.13	
S_H	−0.13		−0.10	

[a]DFT data of MBA SAM on Au(111) obtained either with or without van der Waals (vdW) interactions between MBA molecules. The two MBA molecules in the unit cell are bonded on Au(111) with the S atom located on bridge-fcc hollow (S_F, MBA_F) or bridge-hcp hollow (S_H, MBA_H) sites.

optimized configurations, both with and without van der Waals interactions, is also presented in Table 1. In both cases we have found similar results. The S atoms in the MBA moieties are negatively charged. On the other hand, the topmost surface Au atoms show a differential charge distribution promoted by MBA chemisorption. Au atoms bonded to MBA have removed electronic charge toward the S atom and have a positive charge (red atoms in Figure 4b), whereas the others are negatively charged (white atoms in Figure 4b). The average charge per Au atom in the topmost layer is nearly zero (+0.02).

The distribution of charges on the Au atoms after charge transfer (Figure 4b and Table 1) could explain the absence of vacancy islands on the Au surface. As a matter of fact, repulsive forces between positively charged Au surface atoms have been considered as the cause of ejection of Au atoms,[40,41] which then bind to thiol molecules to form gold–thiolate species. The monatomic gold vacancies produced by this process should be responsible of the vacancy island formation on the Au surface by Ostwald ripening.[5] However, the charge distribution of the topmost Au atoms in the $(\sqrt{3}\times4)$ MBA lattice shows a periodic distribution of alternating positively and negatively charged Au surface atoms, in contrast to the homogeneous positive charge distribution found for alkanethiolates on Au(111). The average Bader charge for Au surface atom is +0.02 in MBA (+0.05 in the case of alkanethiolates on the unreconstructed (111) surface), whereas the RS-Au-RS model gives much higher values for the Au adatom (+0.12/+0.13).[4] Because repulsive forces among metal atoms are smaller than for alkanethiols, adatoms are not likely to be ejected from the surface, and thus vacancy islands (and gold-adatom species) could not be formed for MBA adsorption. The same argument has been used to rationalize the absence of "pits" in heterocyclic thiols like 6-mercaptopurine[24] and 4-mercaptopyridine[25] on Au(111): in these cases, Bader charges of gold atoms have average values similar to that of MBA SAMs.

There is yet another factor that is crucial in determining whether the Au(111) surface will reconstruct or not: the energetic balance between two opposite effects. On the one hand, the amount of released energy per unit cell area (A) by the S-head-Au interaction is $N_{MBA}E_b/A = -0.023$ eV/Å^2, where N_{MBA} is the number of MBA molecules in the $(\sqrt{3}\times4)$ unit cell. Similar results have been obtained for 6-mercaptopurine and 4-mercaptopyridine: $N_{thiol}E_b/A = -0.022$ and -0.015 eV/Å^2, respectively. In contrast, for alkanethiols (methanethiol) on an unreconstructed surface we have obtained $N_{alkanethiol}E_b/A = -0.080$ eV/Å^2.[4] The E_b values considered here do not include van der Waals interactions, as we are interested only in the S–Au interactions.

On the other hand, we can consider the cost to reconstruct the Au(111) terraces to form the Au adatoms required for the RS-Au-RS c(4×2) lattice:

$$E_{rec} = E^{R}_{Au(111)} - E^{U}_{Au(111)} - n_{ad}E^{Au}_{bulk} \quad (3)$$

where $E^{R}_{Au(111)}$ and $E^{U}_{Au(111)}$ correspond to the energy of the reconstructed Au(111) and unreconstructed Au(111) surface, respectively, E^{Au}_{bulk} is the total energy of a bulk Au atom, and n_{ad} is the number of Au adatoms in the surface unit cell. The value of this reconstruction energy per unit cell area is $E_{rec}/A = +0.021$ eV/Å^2 for a c(4×2) lattice with RS-Au-RS moieties. In the case of MBA, 6-mercaptopurine and 4-mercaptopyridine, E_{rec}/A and $N_{thiol}E_b/A$ have very similar absolute values; i.e., gold-adatom release at terraces, which leads to pit formation, is at least a difficult process. On the contrary, for alkanethiols, $|N_{alkanethiol}E_b|/A$ is much larger than E_{rec}/A, thus explaining pit formation on the Au(111) terraces and reconstruction for the Au-adatom surface structure.

CONCLUSIONS

We have studied the self-assembly of MBA on Au(111) surfaces. Results from STM, XPS, electrochemical data, and DFT calculations show that MBA molecules adsorb on the Au(111) surface forming a $(\sqrt{3}\times4)$ lattice of thiolate species. The absence of vacancy islands and the small surface coverage by gold islands are not consistent with Au-adatom models. DFT data show that, although the contribution of the S–Au thiolate bond is relatively weak compared to alkanethiolates, van der Waals forces between aromatic rings make a strong contribution to SAM stabilization. The absence of vacancy islands correlates well with the small positive charge remaining on the Au surface atoms, and also to the low released energy per unit cell area for the S-head-Au adsorption on the Au(111) surface, as recently observed for 6-mercaptopurine and 4-mercaptopyridine.

In summary, although the structural studies on MBA-protected clusters have been essential in the development of thiolate-adatom models, MBA SAMs on Au(111) seem to be formed on the unreconstructed (111) surface, with no evidence of adatom formation. These results raise an interesting point as regards the validity of making a straightforward parallel between the thiol–Au interface in single crystal surfaces and in monolayer protected clusters.

AUTHOR INFORMATION

Corresponding Author

*E-mail: cvericat@inifta.unlp.edu.ar; Phone: +54 221 4257430; Fax: +54 221 4254642.

Notes

The authors declare no competing financial interest.

ACKNOWLEDGMENTS

This work has been financially supported by ANPCyT (PICT 2554) and CONICET (PIP 00362), both from Argentina, and

CTQ2011-24784 MICIIN, Spain. E. P. acknowledges a doctoral fellowship from CONICET-ANPCyT.

REFERENCES

(1) Nuzzo, R. G.; Allara, D. L. *J. Am. Chem. Soc.* **1983**, *105*, 4481−4483.
(2) Love, J. C.; Estroff, L. A.; Kriebel, J. K.; Nuzzo, R. G.; Whitesides, G. M. *Chem. Rev.* **2005**, *105*, 1103−1170.
(3) Castner, D. G.; Ratner, B. D. Biomedical Surface Science: Foundations to Frontiers. In *Frontiers in Surface and Interface Science*; Duke, C. B., Plummer, E. W., Eds.; North Holland: Amsterdam, 2002.
(4) Vericat, C.; Vela, M. E.; Benitez, G.; Carro, P.; Salvarezza, R. C. *Chem. Soc. Rev.* **2010**, *39*, 1805−1834.
(5) Pensa, E.; Cortés, E.; Corthey, G.; Carro, P.; Vericat, C.; Fonticelli, M. H.; Benítez, G.; Rubert, A. A.; Salvarezza, R. C. *Acc. Chem. Res.* **2012**, *45*, 1183−1192.
(6) Bucher, J.-P.; Santesson, L.; Kern, K. *Langmuir* **1994**, *10*, 979−983.
(7) Hayashi, T.; Morikawa, Y.; Nozoye, H. *J. Chem. Phys.* **2001**, *114*, 7615−7621.
(8) Gottschalck, J.; Hammer, B. *J. Chem. Phys.* **2002**, *116*, 784−790.
(9) Yourdshahyan, Y.; Rappe, A. M. *J. Chem. Phys.* **2002**, *117*, 825−833.
(10) Kondoh, H.; Iwasaki, M.; Shimada, T.; Amemiya, K.; Yokoyama, T.; Ohta, T.; Shimomura, M.; Kono, S. *Phys. Rev. Lett.* **2003**, *90*, 066102.
(11) Roper, M. G.; Skegg, M. P.; Fisher, C. J.; Lee, J. J.; Dhanak, V. R.; Woodruff, D. P.; Jones, R. G. *Chem. Phys. Lett.* **2004**, *389*, 87−91.
(12) Maksymovych, P.; Voznyy, O.; Dougherty, D. B.; Sorescu, D. C.; Yates, J. T., Jr. *Prog. Surf. Sci.* **2010**, *85*, 206−240.
(13) Yu, M.; Bovet, N.; Satterley, C. J.; Bengió, S.; Lovelock, K. R. J.; Milligan, P. K.; Jones, R. G.; Woodruff, D. P.; Dhanak, V. *Phys. Rev. Lett.* **2006**, *97*, 166102.
(14) Grönbeck, H.; Häkkinen, H.; Whetten, R. L. *J. Phys. Chem. C* **2008**, *112*, 15940−15942.
(15) Häkkinen, H. *Nat. Chem.* **2012**, *4*, 443−455.
(16) Häkkinen, H.; Walter, M.; Grönbeck, H. *J. Phys. Chem. B* **2006**, *110*, 9927−9931.
(17) Jadzinsky, P. D.; Calero, G.; Ackerson, C. J.; Bushnell, D. A.; Kornberg, R. D. *Science* **2007**, *318*, 430−433.
(18) Walter, M.; Akola, J.; Lopez-Acevedo, O.; Jadzinsky, P. D.; Calero, G.; Ackerson, C. J.; Whetten, R. L.; Grönbeck, H.; Häkkinen, H. *Proc. Natl. Acad. Sci. U. S. A.* **2008**, *105*, 9157−9162.
(19) Creager, S. E.; Steiger, C. M. *Langmuir* **1995**, *11*, 1852−1854.
(20) Barriet, D.; Yam, C. M.; Shmakova, O. E.; Jamison, A. C.; Lee, T. R. *Langmuir* **2007**, *23*, 8866−8875.
(21) Arihara, K.; Ariga, T.; Takashima, N.; Arihara, K.; Okajima, T.; Kitamura, F.; Tokuda, K.; Ohsaka, T. *Phys. Chem. Chem. Phys.* **2003**, *5*, 3758−3761.
(22) Lee, J. R. I.; Willey, T. M.; Nilsson, J.; Terminello, L. J.; De Yoreo, J. J.; van Buuren, T. *Langmuir* **2006**, *22*, 11134−11141.
(23) Schäfer, A. H.; Seidel, C.; Chi, L.; Fuchs, H. *Adv. Mater.* **1998**, *10*, 839−842.
(24) Pensa, E.; Carro, P.; Rubert, A. A.; Benítez, G.; Vericat, C.; Salvarezza, R. C. *Langmuir* **2010**, *26*, 17068−17074.
(25) Ramírez, E. A.; Cortés, E.; Rubert, A. A.; Carro, P.; Benítez, G.; Vela, M. E.; Salvarezza, R. C. *Langmuir* **2012**, *28*, 6839−6847.
(26) Blöchl, P. E. *Phys. Rev. B* **1994**, *50*, 17953.
(27) Blöchl, P. E.; Margl, P.; Schwarz, K. Ab initio molecular dynamics with the projector augmented wave method. In *Chemical Application of Density-Functional Theory*; Brian, B., Laird, R. B. R., Ziegler, Tom, Eds.; American Chemical Society: Washington, DC, 1996; Vol. *629*, pp 54−69.
(28) Kresse, G.; Joubert, D. *Phys. Rev. B* **1999**, *59*, 1758.
(29) Perdew, J. P.; Chevary, J. A.; Vosko, S. H.; Jackson, K. A.; Pederson, M. R.; Singh, D. J.; Fiolhais, C. *Phys. Rev. B* **1992**, *46*, 6671.
(30) Monkhorst, H. J.; Pack, J. D. *Phys. Rev. B* **1976**, *13*, 5188.
(31) Kresse, G.; Furthmüller, J. *Phys. Rev. B* **1996**, *54*, 11169.
(32) Grimme, S. *J. Comput. Chem.* **2006**, *27*, 1787−1799.
(33) Pearson, W. B. *Handbook of Lattice Spacing and Structure of Metals*; Pergamon Press, Inc.: New York, 1958.
(34) Urcuyo, R.; Cortés, E.; Rubert, A. A.; Benitez, G.; Montero, M. L.; Tognalli, N. G.; Fainstein, A.; Vela, M. E.; Salvarezza, R. C. *J. Phys. Chem. C* **2011**, *115*, 24707−24717.
(35) Yang, G.; Liu, G.-y. *J. Phys. Chem. B* **2003**, *107*, 8746−8759.
(36) Azzam, W.; Bashir, A.; Ulrich Biedermann, P.; Rohwerder, M. *Langmuir* **2012**, *28*, 10192−10208.
(37) Kautz, N. A.; Kandel, S. A. *J. Am. Chem. Soc.* **2008**, *130*, 6908−6909.
(38) He, Y.; Borguet, E. *J. Phys. Chem. B* **2001**, *105*, 3981−3986.
(39) He, Y.; Borguet, E. *Faraday Discuss.* **2002**, *121*, 17−25.
(40) Godin, M.; Tabard-Cossa, V.; Miyahara, Y.; Monga, T.; Williams, P. J.; Beaulieu, L. Y.; Lennox, R. B.; Grutter, P. *Nanotechnology* **2010**, *21*, 075501.
(41) Godin, M. *Surface Stress, Kinetics, and Structure of Alkanethiol Self-Assembled Monolayers*. Ph.D. Thesis, McGill University, Montréal, August 2004.